JCTC Journal of Chemical Theory and Computation

Article

pubs.acs.org/JCTC

Estimation of the Ground State Energy of an Atomic Solid by Employing Quantum Trajectory Dynamics with Friction

Bing Gu,[†] Robert J. Hinde,[‡] Vitaly A. Rassolov,[†] and Sophya Garashchuk*[,†]

[†]Department of Chemistry and Biochemistry, University of South Carolina, Columbia, South Carolina 29208, United States

[‡]Department of Chemistry, University of Tennessee, Knoxville, Tennessee 37996, United States

ABSTRACT: Evolution with energy dissipation can be used to obtain the ground state of a quantum-mechanical system. This dissipation is introduced in the quantum trajectory framework by adding an empirical friction force to the equations of motion for the trajectories, which, as an ensemble, represent a wave function. The quantum effects in dynamics are incorporated via the quantum force derived from the properties of this ensemble. For scalability to large systems, the quantum force is computed approximately yet with sufficient accuracy to describe the strongly anharmonic ground state of solid ^{4}He represented by a simulation cell of 180 atoms.

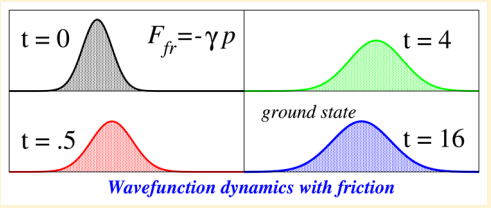

Wavefunction dynamics with friction

1. INTRODUCTION

Solid ^{4}He is an example of a quantum atomic solid, characterized by a large zero-point energy (ZPE), which is beyond the standard methods of analysis based on normal modes. Therefore, computationally intensive methods, such as variational path integral Monte Carlo[1] or quantum diffusion Monte Carlo,[2] are employed to investigate its properties, such as the ground state energy (GSE) and pair-distribution function (PDF).[3−6] Here, we describe an alternative method of estimating the GSE in systems of this type, based on Bohmian or quantum trajectory (QT) dynamics[7] with quantum force and empirical friction.[8] To make the approach practical, the quantum force components are approximated with linear functions on the entire space,[9] and to make it sufficiently accurate, higher-order corrections are added for each atom independently. The approach is applied to study the ground state of solid helium, represented by a simulation cell of 180 atoms, at the density $\varrho = 4.61421 \times 10^3\ a_0^{-3}$ and for the He−He interatomic potential used in refs 3 and 10. The GSE is estimated from the infinite time limit of a wave function energy evolving with the energy dissipation for several values of the friction coefficient. The PDF is computed to further probe the quality of the wave function. The PDF, which can be obtained experimentally from powder diffraction data, gives information about the average structure of a material.[11,12] For a classical solid at absolute zero, the PDF is a set of δ functions at values corresponding to the distance between pairs of atoms. For a quantum solid, these peaks are broadened because of the wave function's delocalization.

Energy dissipation by a system during dynamics is, generally, used to study the interaction of a system with its environment or bath. Theories of system−bath interaction have a long and rich history beyond our scope. The Schrödinger−Langevin equation of Kostin and the Bohmian trajectory implementation of the stochastic Caldirola−Kanai equation by Sanz are most relevant to this work.[13−15] In both approaches, the bath is treated implicitly and is modeled, respectively, through special terms added to the time-dependent Schrödinger equation (TDSE) or, at the loss of ZPE, through the overall damping. To compute the ground state of a system, here we use the TDSE with empirical friction.[8] The formulation is implemented within the QT framework, which makes the addition of the velocity-dependent friction straightforward at the level of equations-of-motion for the QTs (unlike its addition to conventional TDSE).

The remainder of the article is organized as follows: Section 2 describes the QT dynamics with friction and the new two-step approximation to the quantum potential, making the approach scalable to large anharmonic systems. Simulation setup and results for solid ^{4}He are discussed in Section 3, and conclusions are given in Section 4.

2. THEORY

2.1. QT Dynamics with Friction. The quantum or Bohmian trajectory formulation of the TDSE is sketched below, assuming the same mass m for all degrees of freedom (DOFs) described in Cartesian coordinates. A generalization is given in ref 16. Small bold letters denote vectors, and capital bold letters denote matrices whose dimensionality is N_{dim}. In Cartesian coordinates, $N_{\mathrm{dim}} = 3 \times$ (number of atoms) $= 3N_{\mathrm{at}}$. Note that the overhead vector symbol will be used to denote three-dimensional position vectors in Section 3.

The usual TDSE, then, is

$$\hat{H}\psi(\boldsymbol{x},t) = \imath\hbar\frac{\partial}{\partial t}\psi(\boldsymbol{x},t),\ \ \hat{H} = -\frac{\hbar^2}{2m}\nabla\cdot\nabla + V(\boldsymbol{x}) \qquad (1)$$

In the Madelung−de Broglie−Bohm formulation of the TDSE,[17] the wave function is represented in terms of the real amplitude $A(\boldsymbol{x},t)$ and phase $S(\boldsymbol{x},t)$

Received: December 23, 2014
Published: May 20, 2015

DOI: 10.1021/ct501176m
J. Chem. Theory Comput. 2015, 11, 2891−2899

$$\psi(\boldsymbol{x},t) = A(\boldsymbol{x},t)\,\exp\left(\frac{\imath}{\hbar}S(\boldsymbol{x},t)\right) \tag{2}$$

Substitution of eq 2 into eq 1 and definition of the QT momentum as

$$\boldsymbol{p} = \nabla S \tag{3}$$

lead to the following equations of motion for a trajectory

$$\frac{\mathrm{d}\boldsymbol{x}^{(k)}}{dt} = \frac{\boldsymbol{p}^{(k)}}{m} \tag{4}$$

$$\frac{\mathrm{d}\boldsymbol{p}^{(k)}}{\mathrm{d}t} = -\nabla(V+U)|_{x=x^{(k)}} \tag{5}$$

The superscript k labels the trajectories, with their number being N_{traj}, which discretize the initial wave function and, as an ensemble, represent $\psi(\boldsymbol{x},t)$ at all times. The quantum-mechanical features of dynamics enter these classical-like equations of motion via the quantum potential U

$$U(\boldsymbol{x},t) = -\frac{\hbar^2}{2m}\frac{\nabla\cdot\nabla A(\boldsymbol{x},t)}{A(\boldsymbol{x},t)} \tag{6}$$

The quantum potential is nonlocal in $\boldsymbol{x}$ and, being proportional to $\hbar^2/m$, suggests a simple formal transition to classical mechanics: $U \to 0$. The time dependence of the wave function phase along a trajectory, $S^{(k)}$, is defined by

$$\frac{\mathrm{d}S^{(k)}}{\mathrm{d}t} = \frac{\boldsymbol{p}^{(k)}\cdot\boldsymbol{p}^{(k)}}{2m} - (V+U)|_{x=x^{(k)}} \tag{7}$$

In this work, we will also use the so-called nonclassical momentum of a trajectory, defined as

$$\boldsymbol{r} = \frac{\nabla A(\boldsymbol{x},t)}{A(\boldsymbol{x},t)} \tag{8}$$

which evolves according to

$$\frac{\mathrm{d}\boldsymbol{r}^{(k)}}{\mathrm{d}t} = -\left(\boldsymbol{r}^{(k)}\cdot\nabla + \frac{\nabla\cdot\nabla}{2}\right)\frac{\boldsymbol{p}^{(k)}}{m} \tag{9}$$

The derivation of the evolution equations along the QTs (eqs 5, 7, and 9) and of eq 11 are given in the Appendix. The quantum potential can be expressed in terms of the nonclassical momentum

$$U = -\frac{\hbar^2}{2m}(\boldsymbol{r}\cdot\boldsymbol{r} + \nabla\cdot\boldsymbol{r}) \tag{10}$$

(The atomic units of $\hbar = 1$ are used henceforth.) The trajectory weight $w^{(k)}$, which is the probability density within the volume element associated with the kth QT

$$\delta\mathcal{V}^{(k)} = \delta x_1^{(k)}\cdot\delta x_2^{(k)}\cdots\delta x_{N_{\mathrm{dim}}-1}^{(k)}\cdot\delta x_{N_{\mathrm{dim}}}^{(k)}$$

is conserved in time[9] (see the Appendix)

$$w^{(k)} = |\psi(\boldsymbol{x}^{(k)},0)|^2\,\delta\mathcal{V}^{(k)}(0) = |\psi(\boldsymbol{x}^{(k)},t)|^2\,\delta\mathcal{V}^{(k)}(t) \tag{11}$$

Thus, expectation values of the position-dependent operators (and some momentum-dependent operators, such as current density), $\hat{O}$, can be computed using as simple summations over the QT ensemble

$$\langle\hat{O}\rangle = \int|\psi(\boldsymbol{x},t)|^2\,O(\boldsymbol{x})\,\mathrm{d}\mathcal{V} = \sum_{k=1}^{N_{\mathrm{traj}}} O(\boldsymbol{x}^{(k)})w^{(k)} \tag{12}$$

Expectation values are used to analyze the dynamics and, also, to construct approximations to the quantum potential U. Exact computation of U is, in general, unfeasible.[18] The wave function amplitude, $A(\boldsymbol{x},t)$, if needed, can be approximated using the trajectory weights and positions near $\boldsymbol{x}$, but this approximation does not affect evolution of the QT ensemble, i.e., of the wave function itself.[9]

In the trajectory framework, adding momentum-dependent friction to the equations of motion is a straightforward modification of eq 5

$$\frac{\mathrm{d}\boldsymbol{p}^{(k)}}{\mathrm{d}t} = -\nabla(V(\boldsymbol{x}) + U(\boldsymbol{x},t))|_{x=x^{(k)}} - \gamma\boldsymbol{p}^{(k)} \tag{13}$$

The constant $\gamma > 0$ is an empirical friction coefficient. To give physical meaning to the friction force in the context of energy dissipation, i.e., the friction removes energy from the system until the wave function reaches the ground state, the TDSE and the evolution equation for the action function are modified as follows

$$\imath\hbar\frac{\partial}{\partial t}\psi(\boldsymbol{x},t) = \hat{H}\psi(\boldsymbol{x},t) + \gamma(S(\boldsymbol{x},t) - \langle S(\boldsymbol{x},t)\rangle)\,\psi(\boldsymbol{x},t) \tag{14}$$

$$\frac{\mathrm{d}S^{(k)}}{\mathrm{d}t} = \frac{\boldsymbol{p}^{(k)}\cdot\boldsymbol{p}^{(k)}}{2m} - (V+U)|_{x=x^{(k)}} - \gamma(S^{(k)} - \langle S\rangle) \tag{15}$$

From a trajectory-based perspective, energy is being lost from the system due to friction as long as the QTs move; they come to rest when the classical force, $F_{\mathrm{c}} = -\nabla V$, is canceled by the quantum force, $F_{\mathrm{q}} = -\nabla U$, which happens when the QT ensemble describes an eigenstate. Unlike quantum dynamics in imaginary time, which also yields the ground state,[19] dynamics with friction does not change the wave function normalization. For our choice of the friction term, the energy decays with time according to the average kinetic energy of the QTs

$$\frac{\mathrm{d}E}{\mathrm{d}t} = -\frac{\gamma}{m}\langle\boldsymbol{p}\cdot\boldsymbol{p}\rangle \tag{16}$$

The value of γ is chosen by trial with the goal of balancing the propagation time (more time is required if γ is small) and numerical stability (shorter time-steps are required if γ is large). Note that in the QT framework the action function S, corresponding to a stationary wave function, is independent of the trajectory positions $\boldsymbol{x}$, which is reminiscent of the semiclassical stationary action formalism, although the QTs are different from the classical trajectories underlying the semiclassical approaches. A thorough discussion of this issue and a strategy to reconcile Bohmian and semiclassical mechanics are available in a series of papers by Poirier and co-workers.[20]

2.2. Scalability to the High-Dimensionality Approximation of the Quantum Potential. In the QT formulation of the TDSE, all quantum-mechanical effects, such as the ZPE, tunneling, and interference, come from the nonlocal quantum potential, $U(\boldsymbol{x},t)$, given by eq 6 or, equivalently, eq 10, which is added to the external classical potential V in the evolution equations. For anharmonic coupled systems, $U(\boldsymbol{x},t)$, which, in general, is a singular function near the nodes of a wave function,

DOI: 10.1021/ct501176m
J. Chem. Theory Comput. 2015, 11, 2891−2899

is responsible for the complexity of a time-dependent wave function and its exponential scaling with the system size. In the semiclassical regime of dynamics, often appropriate for the nuclei, some simplifications in the structure of wave functions and of the corresponding quantum potentials are expected. Thus, we can use approximations to the quantum potential that scale polynomially with the system's size. The simplest approximation, which is exact for Gaussian wave functions, is a variationally determined linearized quantum force (LQF).[9,21] (Some other approaches to computing the quantum potential are described in refs 22−25.) The LQF is obtained from the first and second moments of $\boldsymbol{x}$, computed over the QT distribution from a single summation over the QT ensemble. The parameters defining an analytical approximate U and the quantum force for all trajectories are determined at every time-step at the cost of a single inversion of a square matrix of the dimension $N_{\mathrm{dim}} + 1$, where N_{dim} is the dimensionality of the system. This cost is negligible compared to the cost of computing the external potential V, often performed on-the-fly, for all but the simplest model potentials.

The LQF is an adequate quantum correction for short-time evolution; the time scale on which the LQF provides a sufficient correction depends on the anharmonicity of the potential. The LQF has been used in recent dynamics studies of a single quantum proton coupled to dozens of classical nuclei forming the active site of an enzyme[26,27] or a graphene flake.[28,29] For dynamics in a highly anharmonic potential of solid helium, however, we have developed a nonlinear quantum force determined in a block-diagonal fashion, which is practical when applied to a simulation cell of 180 quantum atoms.

The variational LQF is defined by the least-squares fit[30] of components of the nonclassical momentum (eq 8) in terms of linear functions of $\boldsymbol{x}$ from minimization of a functional I

$$I = \sum_{i=1}^{N_{\mathrm{dim}}} \langle \| (A^{-1}\nabla A)_i - \tilde{r}_i \|^2 \rangle \tag{17}$$

The subscript i labels the components, or degrees of freedom, of the system, $i = 1, ..., N_{\mathrm{dim}}$. The fitting functions $\tilde{r}_i$ are expansions of the components of the vector $A^{-1}\nabla A$ in a linear basis, $f(\boldsymbol{x}) = \{\boldsymbol{x},1\}$. Minimization is performed with respect to these expansion coefficients, and the optimal coefficients are solutions to the linear matrix equation.[9] The functional I is defined using integration by parts; therefore, its minimization becomes equivalent to the variational definition of U given by eq 10, and the total energy of the system is conserved.

Once $\tilde{\boldsymbol{r}}$ is used in eq 10 instead of $\boldsymbol{r}$, the approximate quantum potential becomes a quadratic function of $\boldsymbol{x}$ that yields a linear quantum force for every trajectory. This approximation is exact for Gaussian wave functions, but it does not presume that $\psi(\boldsymbol{x},t)$ is necessarily a Gaussian wave function.

For an anharmonic system of high dimensionality, the higher-order terms in the quantum force are introduced within a two-step procedure, which is no longer variational but computationally practical.

2.2.1. LSF-1: Global LQF. We perform the least-squares fit of $\boldsymbol{r}$ and $\boldsymbol{p}$ within the linear basis $\boldsymbol{f} = \{\boldsymbol{x},1\}$, i.e., minimize the global (with respect to the degrees of freedom) functionals

$$I_r = \sum_{i=1}^{N_{\mathrm{dim}}} \langle \| (r_i(\mathbf{x},t) - \tilde{r}_i(\mathbf{x},t) \|^2 \rangle \tag{18}$$

$$I_p = \sum_{i=1}^{N_{\mathrm{dim}}} \langle \left\| (p_i(\mathbf{x},t) - \tilde{p}_i(\mathbf{x},t) \right\|^2 \rangle \tag{19}$$

Note that for each degree of freedom r_i and p_i are expanded in all Cartesian coordinates of all atoms. This first step, eq 18, is similar to the LQF of eq 17 except that we now fit the actual values of nonclassical and classical momenta evolved along the trajectories. This step describes the quantum force at the LQF level due to correlation of motion between different nuclei.

2.2.2. LSF-2: Atom-Specific Higher-Order Fit. The residual $\boldsymbol{r}$ and $\boldsymbol{p}$ are fitted with the higher-order polynomials for a single nucleus (referred to as atom) at a time, using the cubic polynomial basis in the degrees of freedom describing only this particular nucleus. Denoting these atom-specific fitting functions with double tilde and the total number of basis functions as N_{bas}, the atom-specific functionals are

$$I_r^{\mathrm{atom}} = \sum_{j\ \mathrm{atom}} \langle \| (r_j(\mathbf{x},t) - \tilde{r}_j(\mathbf{x},t) - \tilde{\tilde{r}}_j(\mathbf{x},t) \|^2 \rangle \tag{20}$$

$$I_p^{\mathrm{atom}} = \sum_{j\ \mathrm{atom}} \langle \| (p_j(\mathbf{x},t) - \tilde{p}_j(\mathbf{x},\ t) - \tilde{\tilde{p}}_j(\mathbf{x},t) \|^2 \rangle \tag{21}$$

The second step adds more flexibility to the approximate quantum potential to account for a non-Gaussian shape of the evolving wave function. The least-squares fit for each nucleus, described in Cartesian coordinates, involves inversion of a matrix of the size N_{bas}. Putting it together, in the presence of friction, the QT dynamics is defined by eqs 4, 9, 13, and 15; the quantum potential is defined by eq 10; and the gradients of $\boldsymbol{r}$ and $\boldsymbol{p}$ are computed analytically from the least-squares fits of these vectors, $\boldsymbol{r} \approx \tilde{\boldsymbol{r}} + \tilde{\tilde{\boldsymbol{r}}}$ and $\boldsymbol{p} \approx \tilde{\boldsymbol{p}} + \tilde{\tilde{\boldsymbol{p}}}$.

2.3. An Example: Two Coupled Quartic Oscillators. To understand the errors of the approximate quantum force in dynamics with friction, let us first examine dynamics of two coupled quartic oscillators for a particle of unit mass $m = 1$ au. The classical potential is given by

$$V(x_1,x_2) = \frac{1}{2}\left(x_1^2 + \frac{1}{2}x_1^4\right) + \frac{1}{2}\left(x_2^2 + \frac{1}{2}x_2^4\right) + \epsilon x_1 x_2 \tag{22}$$

where ϵ is a parameter controlling coupling between the two anharmonic oscillators, set to $\epsilon = {}^1/_2$. The normal modes approximation, i.e., excluding the quartic terms from V, gives $\mathrm{ZPE}^{\mathrm{nm}} = 0.966\ E_{\mathrm{h}}$. Accounting for the quartic terms within first-order perturbation theory gives $\mathrm{ZPE}^{\mathrm{pt}} = 1.432\ E_{\mathrm{h}}$, whereas the exact value is $\mathrm{ZPE}^{\mathrm{ex}} = 1.183\ E_{\mathrm{h}}$. The initial wave function, evolved in time using QTs with friction, is taken as the direct product of the uncoupled harmonic ground states, $\psi(0) = \pi^{-1/2} \exp(-(x_1^2 + x_2^2)/2)$, whose energy is equal to $1.375\ E_{\mathrm{h}}$. Dynamics with the LQF approximation and with the two-step cubic $\boldsymbol{r}/\boldsymbol{p}$-fit approximation are analyzed for the friction constant $\gamma = 6$. QT ensembles of $N_{\mathrm{traj}} = 4800$ were evolved with the time step $\Delta t = 0.002$ au. The total energies, shown on Figure 1 as functions of time, are clearly different. Around $t = 1.5$ au, the wave function energy computed with more accurate quantum force levels off at the ground state value, whereas the energy of the LQF dynamics continues to decrease throughout the propagation. Examination of the QTs at long times shows that the their positions drift toward two regions where the classical force is compensated by the LQF. Figure 2a shows x_1 coordinates of the QTs, which localize near $x_1 = \pm 0.75$ au with time. Fitting with the cubic basis leads to an approximate

DOI: 10.1021/ct501176m
J. Chem. Theory Comput. 2015, 11, 2891−2899

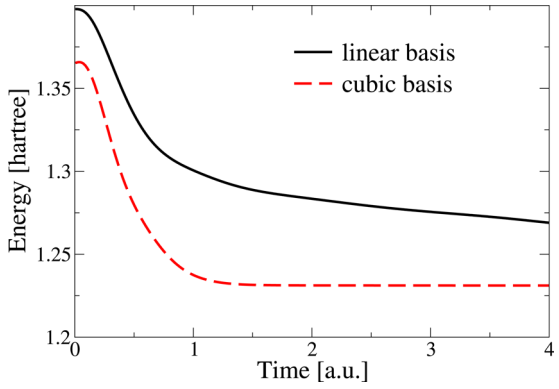

Figure 1. Total energy as a function of time for dynamics of two linearly coupled anharmonic oscillators with the linear basis (LQF, solid line) and cubic basis (dashed line).

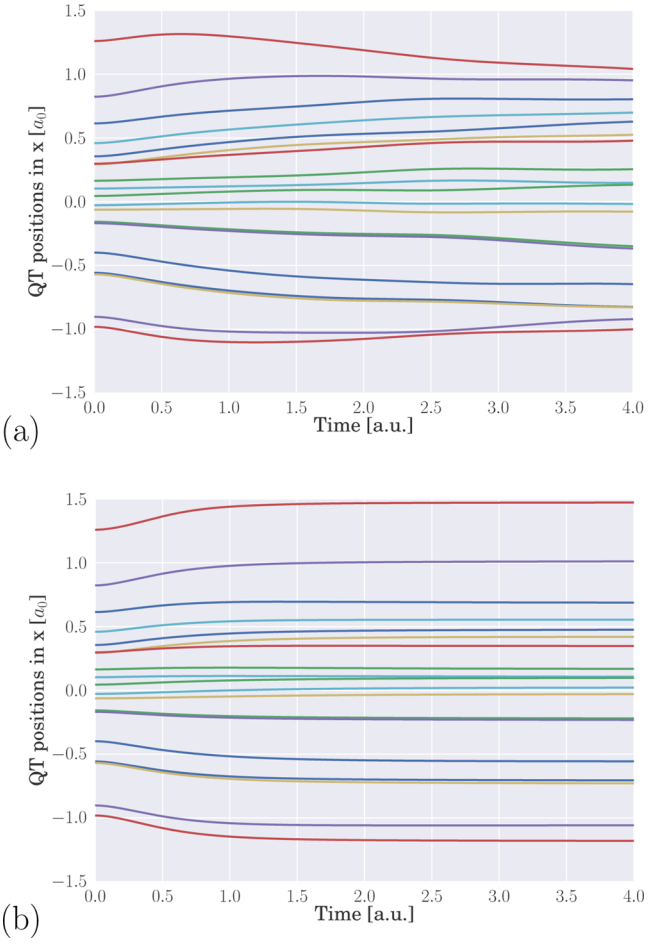

Figure 2. Dynamics of QTs for the coupled anharmonic oscillator with the (a) LQF and (b) cubic basis approximation; x_1 positions of the QTs are shown as functions of time.

quantum force as a fifth-order polynomial, which is sufficiently accurate to cancel the classical force. In this case, QTs become stationary in time, as shown in Figure 2b.

Several snapshots of the quantum potential U and of the combined potential $U + V$ are shown in Figure 3. The main effect of U is to delocalize the wavepacket, as seen in Figure 3a. As time progresses, U and V start canceling each other, as shown in Figure 3b, up to a constant that gives the ZPE. Within the LQF approximation, such cancellation cannot happen because U is limited to a quadratic function at all times. As a result, the LQF trajectories in Figure 2a do not become stationary. In this model, the cubic basis without the cross-term functions $\{x_1x_2, x_1x_2^2, x_1^2x_2\}$ was found to be accurate; thus, the cubic fittings (step LSF-2) were performed separately for each dimension. The ZPE estimate obtained with the two-step cubic fitting of $\boldsymbol{r}$ and $\boldsymbol{p}$ is $\mathrm{ZPE}^{\mathrm{cub}} = 1.23\ E_h$. The discrepancy with the exact value is due to the nonvariational two-step LSF approximation; dissipative dynamics with the variationally determined quantum force, using the same cubic basis, converges with time to $\mathrm{ZPE}^{\mathrm{var}} = 1.18\ E_h$. In general, the accuracy of the approximate quantum force can be assessed from the residual error of the $\boldsymbol{r}$- and/or $\boldsymbol{p}$-fitting given by eqs 20 and 21.

3. GROUND STATE OF SOLID HELIUM

We use the methodology of Section 2 to compute the GSE and PDF of the hexagonally packed solid ^{4}He at the density $\varrho = 4.61421 \times 10^{-3}\ a_0^{-3}$, following the setup and using the classical potential described in ref 3. The simulation cell representing the system consists of 180 helium atoms ($N_{\mathrm{dim}} = 540$) with all of the nuclei treated as quantum particles. In Section 3, for consistency with prior publications of the potential energy, $\vec{r}_j$ with the overhead vector symbol and no italics is used to denote the position of the jth helium nucleus (or atom) expressed by three Cartesian coordinates of the appropriate nucleus out of the full list of $N_{\mathrm{dim}} = 3N_{\mathrm{at}}$ Cartesian coordinates $\boldsymbol{x}$

$$\boldsymbol{x} = (\underbrace{x_1, x_2, x_3}_{\text{atom 1}}, \underbrace{x_4, x_5, x_6}_{\text{atom 2}}, ..., \underbrace{x_{N_{\mathrm{dim}}-2}, x_{N_{\mathrm{dim}}-1}, x_{N_{\mathrm{dim}}}}_{\text{atom } N_{\mathrm{at}}}) \equiv (\vec{r}_1, \vec{r}_2, ..., \vec{r}_{N_{\mathrm{at}}}) \tag{23}$$

where

$$\vec{r}_1 = (x_1, x_2, x_3),\ \vec{r}_2 = (x_4, x_5, x_6), ...,\ \vec{r}_{N_{\mathrm{at}}} = (x_{N_{\mathrm{dim}}-2}, x_{N_{\mathrm{dim}}-1}, x_{N_{\mathrm{dim}}}) \tag{24}$$

3.1. Classical Potential Energy. The potential energy for each configuration is split into the short-range interaction and the long-range interaction, defined by the cutoff distance R_{cut}. The short-range interaction is computed by summing over all interacting pairs (ip)

$$V = \sum_{\mathrm{ip}(i,j)} u(|\vec{r}_{ij}|),\ \vec{r}_{ij} = \vec{r}_j - \vec{r}_i \tag{25}$$

where $\vec{r}_{ij}$ is the time-dependent vector pointing from atom i to atom j, and $u(|\vec{r}|)$ is the interaction between two helium atoms separated by distance $|\vec{r}|$. The He−He pair interaction u is given by the HFD-B(He) potential.[31] The resulting potential as a function of displacement of the central He, shown in Figure 4, for the considered density is strongly anharmonic and of double-well character, which makes methods of analysis based on normal modes invalid. As the density increases, the two minima coalesce at zero displacement and a harmonic approximation to the lattice dynamics becomes more reasonable.

Every atom j in the solid, $j \in [1, N_{\mathrm{at}}]$, has a corresponding lattice site defined by a three-dimensional vector $\vec{R}_j$ similar to eq 24; the separation vector between atoms i and j at lattice sites is $\vec{R}_{ij} = \vec{R}_j - \vec{R}_i$. Periodic boundary conditions and the minimum image convention are used: when computing the

DOI: 10.1021/ct501176m
J. Chem. Theory Comput. 2015, 11, 2891−2899

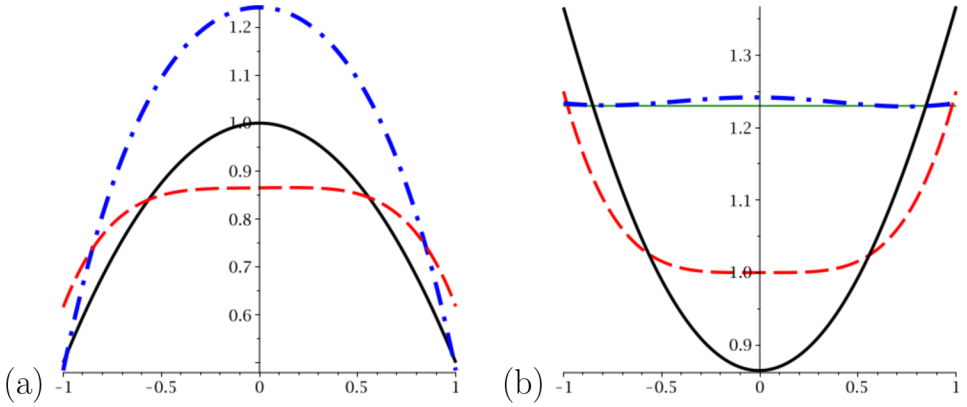

Figure 3. Dynamics of the coupled anharmonic oscillator with the cubic-basis approximation for the quantum potential U. (a) U as a function of x_1 for $x_2 = 0$, computed at $t = \{0,0.5,4\}$ au, is shown as a thick solid line, dashed line, and dot−dashed line, respectively. (b) Sum of the classical and quantum potentials, which generates the forces acting on the trajectories; the thin solid line shows the ZPE estimate at infinite time, and the rest of the legend is the same as that in (a).

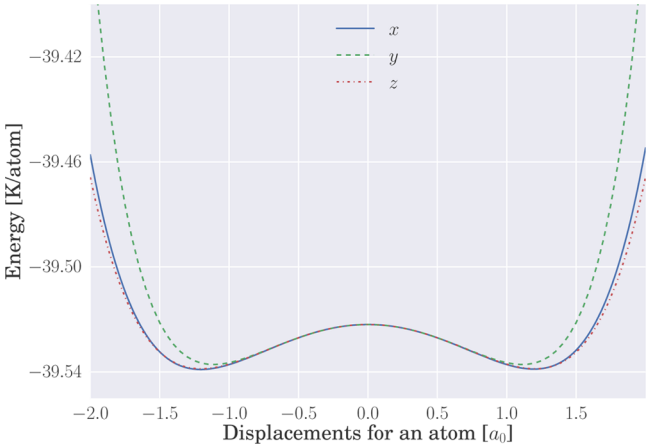

Figure 4. Potential energy as a function of the displacement of the central atom for the 180 atom simulation cell.

distance between atoms i and j including images, the image of j that gives the shortest distance $\vec{R}_{ij}$ is always chosen. A pair is considered to interact if the separation distance satisfies the proximity condition, $|\vec{R}_{ij}| < R_{cut}$. Going through all atoms in the simulation cell, a neighbor list for each atom is created. The neighbor lists are kept fixed, even if the distance between two atoms in an interacting pair becomes larger than R_{cut} during the simulation.

The separation vector $\vec{r}_{ij}$ between two helium atoms labeled i and j, which are generally displaced from their respective lattice sites, can be expressed in terms of the corresponding displacements

$$\vec{r}_{ij} = -\vec{d}_i + \vec{R}_{ij} + \vec{d}_j \tag{26}$$

where $\vec{d}_i = \vec{r}_i - \vec{R}_i$ is the three-dimensional displacement vector for atom i and likewise for j. The two-body potential is computed over a fine grid of squares of the distance between two atoms, and V at any point is computed using linear interpolation between the grid points. The potential is set to a linear function at very short distances. The classical force is computed similarly: the gradients of pairwise interactions are precomputed over the same grid by the finite difference method and summed to yield the total force. Treating V as a function of $|\vec{r}_{ij}|^2$, the gradient of V with respect to the components of the displacement vector $\vec{d}_i$ is

$$\nabla_{\vec{d}_i} V(|\vec{r}_{ij}|^2) = 2 \sum_j (-\vec{d}_i + \vec{R}_{ij} + \vec{d}_j) \frac{\partial V}{\partial |\vec{r}_{ij}|^2} \tag{27}$$

For the value of R_{cut} used in our simulation, the He−He distances were never sufficiently small to neglect with the HFB-D(He) potential.

The long-range interaction is precomputed by the polynomial fitting up to the second order, performed over the three-dimensional grid of displacements of a single helium atom, keeping other atoms at their equilibrium grid positions. The potential energy coming from the long-range interactions is obtained by summing contributions from all pairs whose distance exceeds the cutoff distance R_{cut}, taking into account the periodic boundary conditions. The system size is enlarged until the long-range potential is converged within 10^{-8} E_h. After obtaining $N_{pnt} = N_x \times N_y \times N_z$ values in the three-dimensional Cartesian space (x,y,z) for the long-range part of the potential, V_{lr}, the following matrix equation is solved to obtain the fitting coefficients $\boldsymbol{c} = (c_1,c_2, \ldots,c_{N_{lr}})^T$

$$\boldsymbol{M}^T\boldsymbol{M}\boldsymbol{c} = \boldsymbol{M}^T\boldsymbol{v}_{lr} \tag{28}$$

In eq 28, $\boldsymbol{M}$ is an $N_{pnt} \times N_{lr}$ matrix and N_{lr} is the size of the Taylor basis in the polynomial fit of V_{lr}. For quadratic polynomials, the basis size is $N_{lr} = 10$. The number of points used to fit the long-range part of the potential is $N_{pnt} \approx 40\,000$. For each ith line of $\boldsymbol{M}$ ($i \in [1,N_{pnt}]$), the matrix elements are

$$M_{i,1\ldots N_{lr}} = \{1,x^{(i)},y^{(i)},z^{(i)},x^{(i)}x^{(i)},y^{(i)}y^{(i)},z^{(i)}z^{(i)},x^{(i)}y^{(i)},y^{(i)}z^{(i)},x^{(i)}z^{(i)}\} \tag{29}$$

where $(x^{(i)},y^{(i)},z^{(i)})$ denotes the Cartesian geometry of the ith point. The vector $\boldsymbol{v}_{lr}$ is the column-vector including the long-range interaction values at all displacements

$$(v_{lr})_i = V_{lr}(x^{(i)},y^{(i)},z^{(i)}), \quad i \in [1,N_{pnt}] \tag{30}$$

The long-range force is computed analytically from the polynomial fit of the long-range potential. The potential energy profiles from all short- and long-range contributions are shown in Figure 4.

3.2. Numerical Implementation. The code is implemented in *FORTRAN* and is massively parallelized using message passing interface (MPI). The work flow of the

DOI: 10.1021/ct501176m
J. Chem. Theory Comput. 2015, 11, 2891−2899

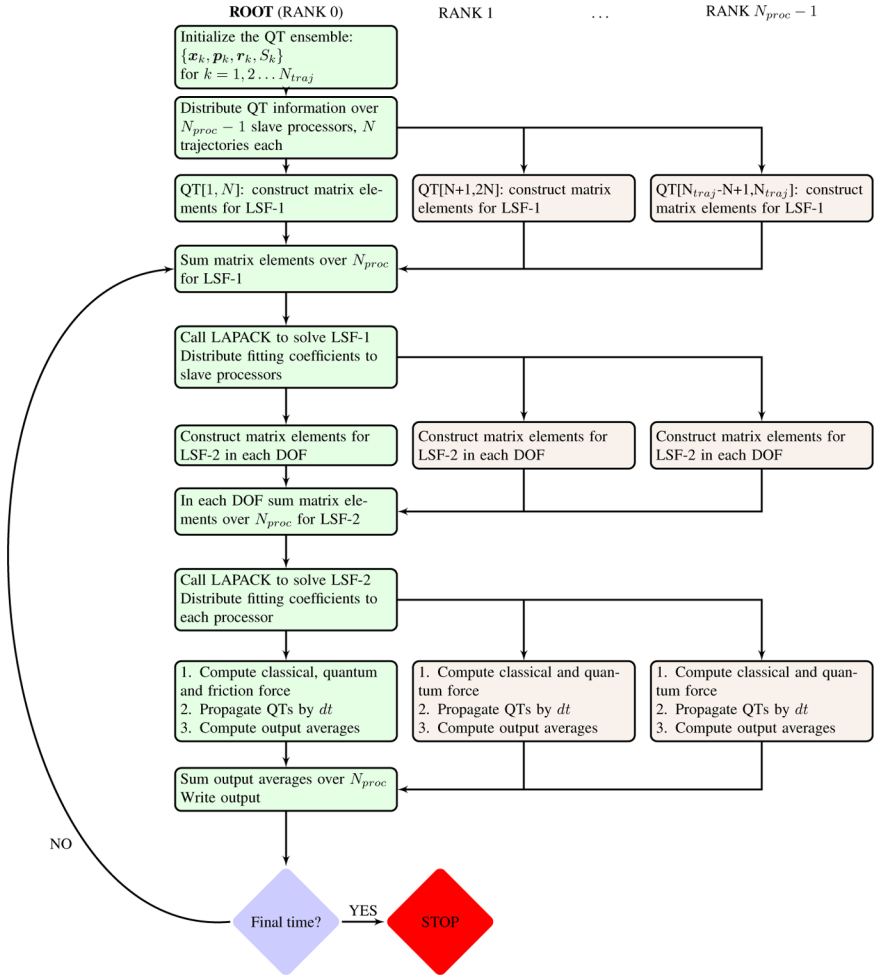

Figure 5. Parallel implementation of approximate QT dynamics with many quantum degrees of freedom. N_{traj} quantum trajectories are equally distributed among N_{proc} processors, $N = N_{\mathrm{traj}}/N_{\mathrm{proc}}$, to compute the classical potential and force, sum over the trajectories for calculation of ensemble averages, and compute the approximate quantum potential and force. DOF, degrees of freedom; LSF, least-squares fit. Systems of linear equations determining the parameters of the ***r***- and ***p***-fit, which determine the quantum correction, are solved on the root processor. LSF-1 is step 1 of Section 2, determining the quantum correction; the correction is found globally, in a basis of linear functions over all DOFs. LSF-2 is step 2 of Section 2, determining the quantum correction for each DOF; this correction is found for ith DOF in a cubic basis $\boldsymbol{f}_i = (1, x_i, x_i^2, x_i^3)$ fitting the residuals $r_i - \tilde{\tilde{r}}_i$ and $p_i - \tilde{\tilde{p}}_i$.

simulation is represented by a diagram in Figure 5. The QTs are initiated with the Monte Carlo sampling of the wave function density using normal deviates[30] in the root processor and then distributed over multiple nodes calling MPI subroutines. Each node is a multiprocessor unit. Computation of the expected values of operators requires information such as $\{\boldsymbol{x}^{(k)}, \boldsymbol{p}^{(k)}, \boldsymbol{r}^{(k)}, S^{(k)}\}$ from all trajectories. In the first step of our approximation to quantum potential, we need to construct a large basis overlap matrix $\boldsymbol{S}$, whose dimension $(N_{\mathrm{dim}} + 1)$ is equal to the size of the LQF basis, $\boldsymbol{f} = (x_1, x_2, \ldots, x_{N_{\mathrm{dim}}}, 1)$. Information regarding all of the trajectories has to be combined to compute the matrix elements (and the output quantities). The matrix elements of $\boldsymbol{S}$ are expected values of position operators

$$S_{ll'} = \sum_{k}^{N_{\mathrm{traj}}} f_l(\boldsymbol{x}^{(k)})\, f_{l'}(\boldsymbol{x}^{(k)})\, w^{(k)} \tag{31}$$

Computation of classical potential and force, involving summations over all interacting pairs, for each QT from the trajectory ensemble is distributed across all N_{proc} processors. Once this has been implemented, we found that passing the trajectory-specific information to the root and construction of the matrix overlap $\boldsymbol{S}$ becomes the computational bottleneck. Therefore, unlike previous implementation of the QT code for a few quantum nuclei,[28] the computation of matrix elements of $\boldsymbol{S}$, as well as all average quantities for the output, is performed on all N_{proc} processors, i.e., the nth processor computes a part $\boldsymbol{S}^{(n)}$ of the overlap matrix. Summation over processors at the root processor give the total $\boldsymbol{S}$, $\boldsymbol{S} = \sum_n^{N_{\mathrm{proc}}} \boldsymbol{S}^{(n)}$. After solving for the LQF parameters of the first step of the ***r***- and ***p***-fitting, using parallel LAPACK, these parameters are passed to the slave processors, and the second step of the fitting is performed by employing the same strategy as that in the first step. To perform the residual ***r***- and ***p***-fitting in the cubic basis, the 4×4 overlap matrices and other average quantities required for the LSF-2 step are constructed for each degree of freedom by partial summation on the slave processors, followed by summation over the processors on the root processor. Then, the least-squares fit equations are solved for each dimension $n \in [1, N_{\mathrm{dim}}]$, and the fitting parameters are passed to the slave processors. The quantum force is computed on each processor

DOI: 10.1021/ct501176m
J. Chem. Theory Comput. 2015, 11, 2891−2899

for a set of trajectories assigned to the processor for the duration of the time propagation, and the trajectory positions, momenta, and action functions are updated. We find that for our system of interest (N_{traj} = 19 200, N_{dim} = 540) numerical efficiency within a fairly simple code structure is achieved when the trajectory information is never passed from the slave processors to the root during the time propagation.

3.3. Results. QT dynamics with friction is applied, following ref 3, to obtain the ground state properties of ^{4}He, which is a hexagonal close-packed (hcp) solid, at density $\varrho = 4.61421 \times 10^{-3}\ a_0^{-3}$, corresponding to molar volume $V_{mol} = 19.34$ cm^3/mol. The nearest-neighbor distance is 6.74223 a_0. The initial wave function is chosen as a product of real Gaussian functions centered at the lattice sites of each atom

$$\psi(\boldsymbol{x},0) = \prod_{i=1}^{N_{dim}} \left(\frac{2\alpha_i}{\pi}\right)^{1/4} \exp(-\alpha_i(x_i - X_i)^2) \tag{32}$$

where $\boldsymbol{X} = (\vec{R}_1, ..., \vec{R}_{N_{at}})$ is the vector of dimension $3N_{dim}$, listing positions of lattice sites of all atoms in the simulation cell, and $\boldsymbol{x}$ is the vector of the coordinates of all the nuclei as stated in eq 23. The Gaussian width parameter is set $\alpha_i = 0.8\ a_0^{-2}$ and the time step dt = 3 au. The friction constant is chosen to have the values $\gamma = 8$ and $\gamma = 40$ to check the dependence of the results on this parameter. The QT ensemble consisted of 19 200 trajectories whose positions randomly sampled $|\psi|^2$ using normal deviates.[30] The simulation parameters are listed in Table 1. Typical runs were executed on N_{proc} = 960 processor on Cray XC30 Darter[32] taking a wall-clock time of about 140 min.

Table 1. Simulation Parameters

simulation cell	5 × 3 × 3
R_{cut}	13.8 a_0
N_{traj}	19 200
N_{dim}	3 × 180
m	4 × 1836 au
γ	{8,40} (au time)$^{-1}$
dt	3 au
$\psi(\boldsymbol{x},t_0)$	Gaussian, eq 32
width α	0.8 a_0^{-2}

To increase numerical efficiency and accuracy, the long-time $E(t)$ is fit with an exponential function

$$E(t) = A \exp(-Bt) + \text{GSE}$$

which gives the GSE estimate from a finite propagation time. The results are given in Table 2 along with those obtained earlier using exact quantum methods; the GSE is reported in units of kelvin per atom; the potential energy of the normal lattice site is −39.52 K/atom. The QT estimates are very close to the results of the path integral approaches.

Table 2. Ground State Energy (GSE) Estimates Obtained from QT Dynamics for Several Values of the Friction Constant γ and Previously Reported Values[a]

method	friction γ	GSE [K/atom]
QT dynamics	12 (au time)$^{-1}$	−5.50
QT dynamics	40 (au time)$^{-1}$	−5.54
quantum path integral[b]		−5.48
diffusion Monte Carlo[c]		−5.50

[a]The time interval $t = [9,12] \times 10^4$ has been used to estimate the GSE from dynamics with friction. [b]The quantum path integral calculation of Hinde.[3] [c]The diffusion Monte Carlo calculation of Cazorla and Boronat.[10]

We further examine the quality of the corresponding ground state wave function by computing the averaged PDF, denoted g_r. The PDF, giving the distribution of distances between the atoms and measuring system disorder, is defined as

$$g(\vec{r}_1,\vec{r}_2) = \frac{N_{at}(N_{at}-1)}{\varrho^2}\,\rho(\vec{r}_1,\vec{r}_2) \tag{33}$$

In eq 33, N_{at} is the number of atoms, and, using $\mathcal{V}$ as the volume, $\varrho = N_{at}/\mathcal{V}$ is the single particle density. The function $\rho(\vec{r}_1,\vec{r}_2)$ is the joint probability

$$\rho(\vec{r}_1,\vec{r}_2) = \int\cdots\int |\psi(\vec{r}_1,\vec{r}_2,...,\vec{r}_{N_{at}})|^2\ \mathrm{d}\vec{r}_3,...,\mathrm{d}\vec{r}_{N_{at}} \tag{34}$$

which is the probability density integrated over the coordinates of all atoms except $j = 1$ and $j = 2$; $\int ...\mathrm{d}\vec{r}_j$ is the three-dimensional integral over the coordinates of atom j. The one-dimensional pair distribution function is obtained by averaging the PDF of eq 33 over the center-of-mass position $\vec{r}_c = (\vec{r}_1 + \vec{r}_2)/2$, the polar angle $\theta = [0,\pi]$, and the azimuthal angle $\phi = [0,2\pi]$

$$g(|\vec{r}_{12}|) = \frac{\int\int\int g(\vec{r}_1,\vec{r}_2)\ \mathrm{d}\vec{r}_c\ \mathrm{d}\phi\ \mathrm{d}(\cos\theta)}{\int \mathrm{d}\vec{r}_c \int \mathrm{d}\phi \int \mathrm{d}(\cos\theta)} \tag{35}$$

Since the wave function is represented by an ensemble of quantum trajectories, it is convenient to recast eq 35 in terms obtainable directly from the trajectories

$$g_r = \int g(|\vec{r}_{12}|)\ \delta(|\vec{r}| - |\vec{r}_{12}|)\ \mathrm{d}|\vec{r}_{12}| = \frac{N_{at}(N_{at}-1)}{\varrho^2}\frac{1}{4\pi\mathcal{V}} \times \int\cdots\int \rho(\vec{r}_1,\vec{r}_2)\delta(|\vec{r}| - |\vec{r}_{12}|)\ \mathrm{d}\vec{r}_c\ \mathrm{d}\phi\ \mathrm{d}(\cos\theta)\ \mathrm{d}|\vec{r}_{12}| \tag{36}$$

Noticing that $\mathrm{d}\vec{r}_{12} = |\vec{r}_{12}|^2\ \mathrm{d}|\vec{r}_{12}|\ \mathrm{d}\phi\ \mathrm{d}(\cos\theta)$ and substituting it into eq 36, we obtain

$$g_r = \frac{N_{at}-1}{4\pi\varrho}\left\langle \frac{\delta(|\vec{r}| - |\vec{r}_{12}|)}{|\vec{r}_{12}|^2} \right\rangle \tag{37}$$

Here, $\langle ... \rangle$ represents an average over the QT ensemble. Numerically, a histogram for pair distribution function g_r over a range $[R_{min},R_{max}]$ is computed over a finite number of intervals.

Figure 6 shows the pair distribution function computed at the density $\varrho = 5.231 \times 10^{-3}\ a_0^{-3}$. The value is chosen such that we can compare our results to those obtained using variational path integral molecular dynamics of Miura.[4] The two peaks in the PDF are in good agreement with Miura's results considering both the position of peaks and their intensity, even though we are using different pair interaction. To explore the ground state wave function further, we have computed PDFs for artificial atomic masses. ^{3}He has a slightly wider peaks in the PDF, which is expected since the wave function should be more delocalized for lighter particles. Using a mass of 8 × 1836 au., we see a sharper first peak, which is closer to the classical picture. The ground state is more localized or ordered while having a heavier atom and is more disordered with a lighter atom, as expected.

DOI: 10.1021/ct501176m
J. Chem. Theory Comput. 2015, 11, 2891−2899

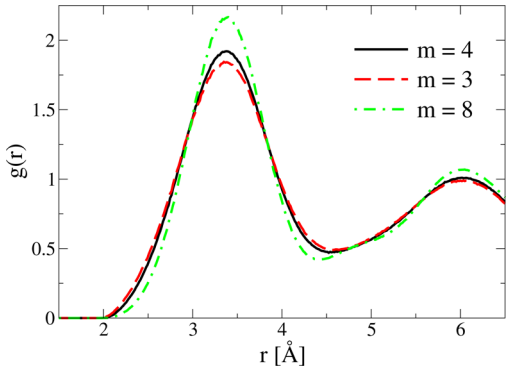

Figure 6. Pair distribution function g_r for the atomic mass m = 4 of ^{4}He and for the fictitious masses of m = 3 and m = 8.

4. CONCLUSIONS

We have described a general approach of finding the vibrational ground state of high-dimensional quantum systems from the quantum trajectory dynamics with dissipation and its first application to a quantum solid described by a simulation cell of 180 atoms, or 540 degrees of freedom. A nuclear wave function is represented by a trajectory ensemble evolving in time under the influence of the external classical potential, approximate quantum potential, and empirical friction. Scalability to hundreds of degrees of freedom is possible due to a globally determined approximation to the quantum force. Effects of interatomic coupling is described within the linearized quantum force approximation requiring single inversion of the $(N_{\mathrm{dim}} + 1) \times (N_{\mathrm{dim}} + 1)$ matrix per time step. Adequate accuracy is achieved from subsequent cubic polynomial fitting of the nonlinear part of the classical and nonclassical momenta based on N_{dim} inversions of 4×4 matrices. In our application to solid helium, inclusion of the nonlinear terms into the least-squares fits for each degree of freedom independently were found to be sufficiently accurate.

For more general anharmonic systems, such fitting can be performed for individual nuclei (3 degrees of freedom at a time) or even atoms with nearest neighbors (on the order of 21 degrees of freedom at a time). Fitting with high-order polynomials over hundreds of dimensions at once will quickly become prohibitively expensive due to matrix size and due to increasing number of QTs. However, high-order correlations between distant particles are likely to be quenched with increasing system size. Massively parallel implementation of the QT dynamics with friction, including both (i) the two-step calculation of the quantum force and (ii) computation of the classical potential and its gradient, was essential for the study of the solid helium system.

Our simulations of solid ^{4}He gave GSEs in agreement to better than 1% for the empirical friction constants within a range γ = [8,40] (au time)$^{-1}$ and compared to previously reported values obtained with quantum path integral approaches for the same interatomic potential. The number of potential energy evaluations performed for a single calculation described in Section 3 is about 80% of a single run in the earlier work of Hinde[3] (7.7×10^{12} compared to 9.5×10^{12} He–He pair-potential evaluations). The ground state wave function was further examined by calculating the pair distribution function for ^{4}He, which was found to be in good agreement with the results of Miura (for a different pair-interaction potential). The PDF for two fictitious isotopes of He exhibited the expected trend: delocalization of the ground state wave function or disorder of the quantum system at zero temperature due to the GSE becomes less significant with increasing particle mass. Future research will include conceptual development and simulations needed for the analysis of vibrational modes using correlation functions.[33,34]

APPENDIX

Time-Evolution Equations of the Quantum Trajectory Dynamics

To simplify notations in this section, subscripts i and j will be used to indicate the Cartesian components of vectors, which range from 1 to N_{dim} in sums and products; the arguments of the functions, $\psi \equiv \psi(\boldsymbol{x},t)$ and so on, will be suppressed. Substitution the wavefunction in the form given by eq 2 into the TDSE (eq 1) and division by ψ leads to the following evolution equations for the wave function amplitude and phase

$$\frac{\partial A}{\partial t} = -\frac{\boldsymbol{p}\cdot\nabla A}{m} - \frac{A\nabla\cdot\boldsymbol{p}}{2m} \tag{38}$$

$$\frac{\partial S}{\partial t} = -\frac{\boldsymbol{p}\cdot\boldsymbol{p}}{2m} - V - U \tag{39}$$

where U is the quantum potential of eq 6. The quantum or Bohmian trajectory is defined by equating its momentum to the gradient of the wave function phase $\boldsymbol{p} = \nabla S$, whose position changes according to $\mathrm{d}\boldsymbol{x}/\mathrm{d}t = \boldsymbol{p}/m$, as given in eq 4. The full time-derivative $\mathrm{d}/\mathrm{d}t$ is used for the functions associated with the quantum trajectories (Lagrangian frame of reference); the partial time derivative $\partial/\partial t$ refers to the functions defined in the stationary, Eulerian frame of reference. Transformation of the Hamilton–Jacobi eq 39 to the Lagrangian frame of reference

$$\frac{\mathrm{d}}{\mathrm{d}t} = \frac{\partial}{\partial t} + \frac{\boldsymbol{p}}{m}\cdot\nabla \tag{40}$$

gives eq 7, while the same transformation of the gradient of eq 39 gives eq 5, defining evolution of the action function and the trajectory momentum, respectively.

Now let us turn to the time evolution of the wave function amplitude A. Multiplying eq 38 by $2A$ and transformation to the Lagrangian framework gives the time dependence of the probability density, $\rho = A^2$, along a trajectory

$$\frac{\mathrm{d}\rho}{\mathrm{d}t} = -\frac{\rho}{m}\nabla\cdot\boldsymbol{p} \tag{41}$$

Equation 41 is the continuity equation for ρ. The time dependence of the volume element, associated with each trajectory, $\delta\mathcal{V} = \Pi_j \delta x_j$, according to $\mathrm{d}\boldsymbol{x}/\mathrm{d}t = \boldsymbol{p}/m$, is defined for each component as $\mathrm{d}(\delta x_j)/\mathrm{d}t = \delta p_j/m$

$$\frac{\mathrm{d}}{\mathrm{d}t}\delta\mathcal{V} = \frac{\mathrm{d}}{\mathrm{d}t}\Pi_j \delta x_j = \sum_j \delta p_j \Pi_{i\neq j}\delta x_i = \sum_j \frac{\delta p_j}{\delta x_j}\Pi_i \delta x_i$$
$$= \delta\mathcal{V}\nabla\cdot\boldsymbol{p} \tag{42}$$

From eqs 41 and 42, it follows that the trajectory weights, $w = \rho\delta\mathcal{V}$, are constant in time, $\mathrm{d}(\rho\delta\mathcal{V})/\mathrm{d}t = 0$, which proves eq 11.

To obtain eq 9, let us divide eq 38 by A and rearrange the terms as follows

DOI: 10.1021/ct501176m
J. Chem. Theory Comput. 2015, 11, 2891–2899

$$\frac{\partial(\ln A)}{\partial t} = -\frac{1}{m}\boldsymbol{p}\cdot\boldsymbol{r} - \frac{1}{2m}\nabla\cdot\boldsymbol{p} = -\frac{1}{m}\sum_j p_j r_j - \frac{1}{2m}\sum_j \frac{\partial p_j}{\partial x_j} \quad (43)$$

where

$$r_i = \frac{1}{A}\frac{\partial A}{\partial x_i},\ p_i = \frac{\partial S}{\partial x_i} \quad (44)$$

Differentiating eq 43 with respect to x_i and switching the order of differentiation on the left-hand side, one obtains

$$m\frac{\partial r_i}{\partial t} = -\sum_j \frac{\partial p_j}{\partial x_i} r_j - \sum_j p_j \frac{\partial r_j}{\partial x_i} - \frac{1}{2}\sum_j \frac{\partial^2 p_j}{\partial x_j\,\partial x_i} \quad (45)$$

Using the definitions of eq 44

$$\frac{\partial r_j}{\partial x_i} = \frac{\partial^2(\ln A)}{\partial x_i\,\partial x_j} = \frac{\partial r_i}{\partial x_j},\quad \frac{\partial p_j}{\partial x_i} = \frac{\partial^2 S}{\partial x_i\,\partial x_j} = \frac{\partial p_i}{\partial x_j} \quad (46)$$

Transformation to the Lagrangian framework (eq 40) eq 45 and replacing p_i and r_i with the corresponding vectors, $\boldsymbol{p}$ and $\boldsymbol{r}$, respectively, makes eq 45 equivalent to eq 9

$$m\frac{\mathrm{d}\boldsymbol{r}}{\mathrm{d}t} = -\sum_j r_j\frac{\partial \boldsymbol{p}}{\partial x_j} - \frac{1}{2}\sum_j \frac{\partial^2 \boldsymbol{p}}{\partial x_j\,\partial x_j} = -\left(\mathbf{r}\cdot\nabla + \frac{1}{2}\nabla\cdot\nabla\right)\boldsymbol{p} \quad (47)$$

AUTHOR INFORMATION

Corresponding Author

*E-mail: garashchuk@sc.edu.

Funding

This material is based on work partially supported by the National Science Foundation under grant no. CHE-1056188. XSEDE allocation TG-DMR110037 time on Darter at the National Institute for Computational Sciences and use of USC HPC cluster funded by the National Science Foundation under grant no. CHE-1048629 are also acknowledged. V.A.R. acknowledges partial support by the National Science Foundation under grant no. CHE-1213604. R.J.H. acknowledges partial support by the National Science Foundation under grants no. CHE-0848841 and CHE-1362520.

Notes

The authors declare no competing financial interest.

REFERENCES

(1) Ceperley, D. M. *Rev. Mod. Phys.* **1995**, *67*, 279−355.
(2) Anderson, J. B. *J. Chem. Phys.* **1975**, *63*, 1499−1503.
(3) Hinde, R. J. *Comput. Phys. Commun.* **2011**, *182*, 2339−2349.
(4) Miura, S. *Comput. Phys. Commun.* **2011**, *182*, 274−276.
(5) Hansen, J.-P.; Levesqure, D. *Phys. Rev.* **1968**, *165*, 293−299.
(6) Hansen, J. P.; Pollock, E. L. *Phys. Rev. A* **1972**, *5*, 2651−2665.
(7) Wyatt, R. E. *Quantum Dynamics with Trajectories: Introduction to Quantum Hydrodynamics*; Springer-Verlag: New York, 2005.
(8) Garashchuk, S.; Dixit, V.; Gu, B.; Mazzuca, J. *J. Chem. Phys.* **2013**, *138*, 054107.
(9) Garashchuk, S.; Rassolov, V. A. *J. Chem. Phys.* **2004**, *120*, 1181−1190.
(10) Cazorla, C.; Boronat, J. *J. Phys.: Condens. Matter* **2008**, *20*, 015223.
(11) Levashov, V. A.; Billinge, S. J. L.; Thorpe, M. F. *J. Comput. Chem.* **2007**, *28*, 1865−1882.
(12) Chandler, D. *Introduction to Modern Statistical Mechanics*; Oxford University Press: New York, 1987.
(13) Kostin, M. D. *J. Chem. Phys.* **1972**, *57*, 3589−3591.
(14) Kanai, E. *Prog. Theor. Phys.* **1948**, *3*, 440−442.
(15) Sanz, A. S.; Martinez-Casado, R.; Penate-Rodriguez, H. C.; Rojas-Lorenzo, G.; Miret-Artes, S. *Ann. Phys.* **2014**, *347*, 1−20.
(16) Rassolov, V. A.; Garashchuk, S.; Schatz, G. C. *J. Phys. Chem. A* **2006**, *110*, 5530−5536.
(17) Bohm, D. *Phys. Rev.* **1952**, *85*, 166−193.
(18) Rassolov, V. A.; Garashchuk, S. *Chem. Phys. Lett.* **2008**, *464*, 262−264.
(19) Kosloff, R.; Tal-Ezer, H. *Chem. Phys. Lett.* **1986**, *127*, 223−230.
(20) Poirier, B. *J. Chem. Phys.* **2004**, *121*, 4501−4515.
(21) Garashchuk, S.; Rassolov, V. A. *Chem. Phys. Lett.* **2003**, *376*, 358−363.
(22) Goldfarb, Y.; Degani, I.; Tannor, D. J. *J. Chem. Phys.* **2006**, *125*, 231103.
(23) Wyatt, R. E.; Bittner, W. R. *J. Chem. Phys.* **2000**, *113*, 8898−8907.
(24) Kendrick, B. K. *J. Chem. Phys.* **2003**, *119*, 5805−5817.
(25) Trahan, C. J.; Hughes, K.; Wyatt, R. E. *J. Chem. Phys.* **2003**, *118*, 9911−9914.
(26) Mazzuca, J.; Garashchuk, S.; Jakowski, J. *Chem. Phys. Lett.* **2012**, *542*, 153−158.
(27) Mazzuca, J. W.; Garashchuk, S.; Jakowski, J. *Chem. Phys. Lett.* **2014**, *613*, 104−109.
(28) Garashchuk, S.; Jakowski, J.; Wang, L.; Sumpter, B. G. *J. Chem. Theory Comput.* **2013**, *9*, 5221−5235.
(29) Wang, L.; Jakowski, J.; Garashchuk, S. *J. Phys. Chem. C* **2014**, *118*, 16175−16187.
(30) Press, W. H.; Flannery, B. P.; Teukolsky, S. A.; Vetterling, W. T. *Numerical Recipes: The Art of Scientific Computing*, 3rd ed; Cambridge University Press: Cambridge, 2007.
(31) Aziz, R.; McCourt, F.; Wong, C. *Mol. Phys.* **1987**, *61*, 1487.
(32) Darter is a supercomputer at the National Institute of Computational Sciences. It is a Cray XC30 system with an Aries interconnect and a Lustre storage system.
(33) Mazenko, G.; Banavar, J.; Gomer, R. *Surf. Sci.* **1981**, *107*, 459−468.
(34) Boon, J.-P.; Yip, S. *Molecular Hydrodynamics*; Dover Publications: New York, 1991.

DOI: 10.1021/ct501176m
J. Chem. Theory Comput. 2015, 11, 2891−2899